Specialized Finite Element Analysis Computer Software for Modeling Hemodynamics in Abdominal Aortic and Carotid Artery Bifurcation Aneurysms

Vijayajothi Paramasivam
Faculty of Science and Technology
Open University Malaysia
Malaysia

Kanesan Muthusamy
Faculty of Science and Technology
Open University Malaysia
Malaysia

Nenad Filipovic
Harvard School of Public Health
Boston MA 02115
USA

ABSTRACT

The developed computer software system is particularly suitable for three dimensional investigations of hemodynamic conditions in abdominal aortic and carotid artery bifurcation aneurysms. It consists of two major clinically relevant modeling scope; rigid wall and deformable wall models. It provides an integrated set of tools that help solve clinically relevant hemodynamic variables such as velocity, wall shear stress and pressure profiles that aids in predicting disease development. The developed graphical user interface is essential for creating mathematical models of an aneurysm with prescribed boundary and initial conditions. This user-friendly interface automatically performs geometric model constructions, input data preparations, model discretizations, computational modeling and post-processing options of the aneurismal models. The blood flow dynamics is defined according to the incompressible Navier-Stokes and the continuity equations for viscous fluids. The computational modeling technique is based on finite element method. Because of the increasing size and complexity of the analysis and the software system design to date, a change in the programming approach and a shift in software design strategy have been proposed for developing readable, expandable and maintainable software systems. This change is from the procedure-oriented to object-oriented programming system development methodologies.

Keywords

Computer software; object-oriented programming; three dimensional finite element analysis; hemodynamic; abdominal aortic aneurysm; carotid artery bifurcation aneurysm

1. INTRODUCTION

The main causes of aneurysm are arteriosclerosis and cystic medial degeneration, but also genetic disorder, malfunction of the aorta (i.e. biomechanical phenomenon), mycotic infections or arthritis can be a cause of aneurysm [1]. Another cause of aneurismal disorders mentioned by scientists is the loss of distensibility of the vessels. Loss of distensibility or increased stiffness of the vessel wall is due to the loss of elastin and increase in collagen content in the aortic wall. This loss is a general result of aging.

Abdominal aortic aneurysm (AAA) is a dilatation of the infrarenal abdominal aorta that lies between the renal bifurcation and the iliac branches. This pathologic condition has been found to affect 8.8% of the population over the age of 65 and if left untreated it may lead to rupture [2]. The size

of the aneurysm and its rate of expansion are parameters widely associated with the risk of rupture [3]. The decision for surgical intervention for patients with aneurysms is complicated because of the lack of a sufficiently accurate rupture risk index. Based on the results from a number of clinical studies, the maximum/peak transverse diameter (PTD) is widely used [4-7]. In cases where PTD exceeds 5 cm – 6 cm, surgical or endovascular treatment is advised.

After heart disease and cancer, the third most common cause of death is stroke. Probably the most frequent stroke is of the embolic type with a heart disease as the source. The carotid bifurcation stenosis is also a significant cause of stroke, producing the infarction in the carotid region by embolization or thrombosis at the site of narrowing. The thrombosis development and embolization is conditioned by the local hemodynamic that can be investigated experimentally and/or by computer modeling [8].

The carotid artery stenosis has a number of risk factors in common with other atherosclerotic diseases. In general, increase of stroke risk is induced by many factors: age, systolic and diastolic hypertension, diabetes, cigarette smoking, etc. Changes of the geometrical vessel dimensions in the region of the carotid artery bifurcation certainly affect the blood flow and may lead to stenosis process. It has been shown that the vessel diameter at the carotid artery bifurcation changes considerably with age.

The shape of aneurysm is very important. The severity of aneurysm is commonly estimated in clinical practice by considering its maximal diameter. However, from the mechanical point of view, the hemodynamic effects and the mechanical stresses within the aneurismal tissue certainly are important in the process of the aneurismal rupture. Bulge diameter alone may not be sufficient criterion for determination of rupure risk, therefore an insight into the hemodynamic effects and the stress-strain quantification and distribution within the vessel wall are of great significance even in medical practice. It is believed that only through the creation of biomechanics based models that it is possible to develop realistic surgical simulators that allow clinicians as well as biomedical engineers to explore, analyze, and optimize the biomechanical consequences of surgery in a computer environment before stepping into the operating room. An ideal simulator for the aneurysm should allow the surgeon to investigate the consequences of surgical options, before performing the operation. A simulator with these characteristics requires the finite element analysis capabilities

because of the complex patient-specific nature of the blood flow through the aneurysm.

To develop a realistic numerical simulation of the blood flow through the aneurismal models, it is necessary to model geometry of the aneurysm, incorporate the fluid properties of the blood, calculate this complex system by using the finite element method, perform detailed post-processing of the computed results and create the report for the clinicians. This system of integrated software for quick creation of complex geometric model is presented in this work. The system consists of the automatic finite element mesh generator, the finite element solver and the scientific visualizer. Each part of the system represents an independent modulus organized in the object-oriented environment.

Because of the increasing size and complexity of the analysis and the software system design, a change in the programming approach and a shift in software design strategy have been proposed for developing readable, expandable and maintainable software systems. The change is from the procedure-oriented to object-oriented programming, and this shift is towards the object-oriented system development methodologies.

2. MATERIAL AND METHODS

2.1 Modeling of Abdominal Aortic Aneurysm

2.1.1 Generation of finite element model

A simplified geometry of an aneurysm is shown in Fig. 1. With this software the three dimensional finite element model for the blood flow domain can be parametrically generated. Transition smoothness between the surfaces is achieved by using Bezier's curves. The results can also be displayed with a user-friendly menu in such a way suitable for an insight into medical aspects of the blood flow conditions. A detailed description of the geometric parameters is given in the caption of Fig. 1. The three dimensional finite element models consisting of 8 node brick element (i. e. rectangular element) was used for this three-dimensional analysis.
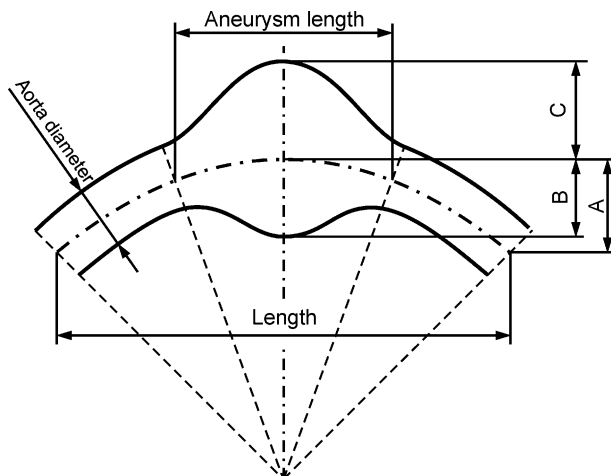

Fig. 1 Geometrical parameters of AAA: 'Length' is the parameter which defines the total horizontal projection of the generated aneurysm model; 'A' is the height of the arc of central line; 'Aorta diameter' is the abdominal aorta diameter; 'B' is the radius from the central line to the inner wall of the aneurysm; 'C' is the radius from the central line to the outer

wall of the aneurysm; 'Aneurysm length' is an average length of the AAA.

2.1.2 Boundary conditions

At the inflow aorta cross-section a fully developed parabolic flow is assumed, determined by a selected volume flux. The normal stress and tangential stress are set to be equal to zero (stress-free condition) or they are prescribed at the outlet cross-section. It is assumed that the entering flow is pulsatile, with a typical waveform shown in Fig. 2 [9]. This waveform can be changed in this software according to ones need to cater for various representation of the Reynolds number of the blood flow.
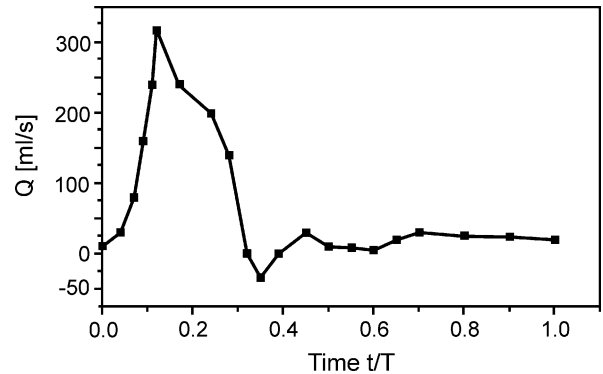

Fig. 2 A typical inflow waveform at the aorta entry. Q is the volumetric in-flux and t/T is the relative time with respect to the cycle period *T*.

2.2 Modeling of Carotid Artery Bifurcation

2.2.1 Generation of finite element model

A simplified carotid artery bifurcation geometry is shown in Fig. 3. The geometric parameters are used for the generation of the blood vessel internal surfaces, which are the boundaries for the blood flow domain. It is assumed that the cross-sections of all arteries are circular, with a transitional region at the branching. With the use of these geometric parameters, a three dimensional finite element model for the blood flow domain is generated as shown in Fig. 4(a). It is assumed that the bifurcation has the symmetry plane (the plane shown in Fig. 3), hence the finite element model is generated for the half of the entire domain (part in front of the symmetry plane). The calculation is performed for this half, but the results are presented for the entire domain.
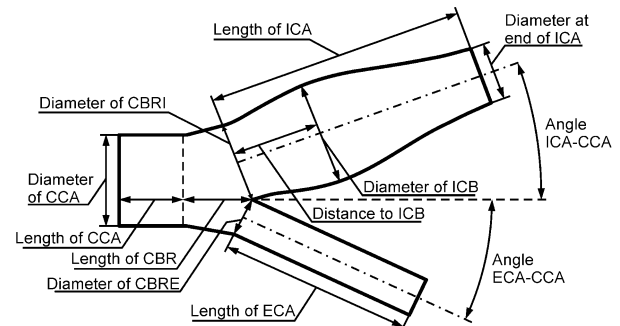

Fig. 3 Geometrical data for the carotid artery model. The abbreviations here are: CCA –common carotid artery, CBR – carotid bifurcation region, CBRE – carotid bifurcation region external, ECA- external carotid artery, CBRI- carotid bifurcation region internal, ICA- internal carotid artery, and ICB- internal carotid bulbus.
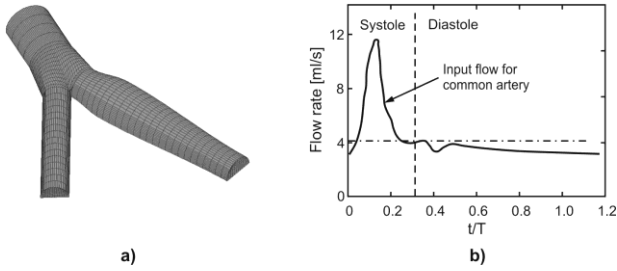
Fig. 4 Finite element model of the carotid artery bifurcation. **a)** Finite element mesh generated using the parameters shown in Fig. 3. The blood flow domain is modeled by three dimensional fluid finite elements; **b)** Flow rate of the blood entering CCA in terms of the relative time t/T, where T is the cycle.

2.2.2 Boundary conditions

At the inflow of CCA a fully developed flow is assumed. The inflow is pulsatile in character and is defined by volumetric blood flow rate Q [*mL*/s] at the common artery entering cross-section. The flow rate is specified by a waveform as shown in Fig. 4(b) [10]. At the fixed walls all velocity components are set to be zero. Also, the velocity components at the plane of symmetry in the direction normal to the plane are set to zero. It is assumed that the end cross-sections of the internal and external carotid arteries are stress-free, i.e. normal and tangential stresses are set to zero. This boundary condition does not represent the real flow conditions at the outflow boundaries, but, by varying the artery lengths, the physiological resistance to the blood flow in the region close to the bifurcation can be matched.

3. THEORY

3.1 Governing Equations of Blood Flow Modeling

The complexity of the cardiovascular system features a tremendous variety of domains such as large arteries, vases of medium caliber as well as capillaries. Their sizes range from few centimeters in diameter down to few micrometers. Except for the very tiny capillaries, the blood flow can be assumed to behave as a continuum [11-13], as well as incompressible, apart from severe pathological situations. As such, its macroscopical behavior can be described by its velocity and pressure fields, related by the mass and momentum conservation laws.

3.1.1 Incompressible viscous fluid flow for rigid wall models

The three-dimensional governing equations (momentum and continuity equations) of a viscous incompressible Newtonian fluid (blood) flow, using the indicial notations with the usual summation convention are, respectively;

$$\rho\left(\frac{\partial v_i}{\partial t} + v_j v_{i,j}\right) = -p_{,i} + \mu v_{i,jj} + f_i^B \quad (1)$$

$$v_{i,i} = 0 \quad (2)$$

where v_i is velocity of blood flow in direction x_i, and summation is assumed on the repeated (dummy) indices, i, j =

1, 2, 3. ρ, p, μ, and f_i^B are the fluid density, fluid pressure, dynamic viscosity of fluid and body force, respectively.

3.1.2 Incompressible viscous fluid flow for deformable wall models

In order to numerically solve fluid flow problems with large displacements of the boundaries such as the deformable wall aneurysm models, one of the most attractive approaches is the arbitrary Lagrangian-Eulerian (ALE) formulation. It is specifically suitable for the fluid-structure interaction (FSI) problems because the moving mesh of the fluid domain can be attached to the structural boundary and the compatibility between the fluid and the solid domains can be conveniently handled.

The governing equations, which includes the Navier-Stokes equations of balance of linear momentum and the continuity equations, is written in the ALE form as;

$$\rho\left[v_i^* + \left(v_j - v_j^m\right)v_{i,j}\right] = -p_{,i} + \mu v_{i,jj} + f_i^B \quad (3)$$

$$v_{i,i} = 0 \quad (4)$$

where * denotes the mesh-referential time derivative i.e. the time derivative at a considered point on the mesh,

$$(\ )^* = \left.\frac{\partial(\ )}{\partial t}\right|_{\xi_i=constant} \quad (5)$$

$$v_{i,i} = 0 \quad (6)$$

where ξ_i is the corresponding point on the mesh.

3.1.3 Mechanical models of blood

Due to complex behavior of blood as a fluid, there are several blood models, which are related to real flow in arteries. The complex rheological properties of blood can be approximated by some of the nonlinear non-Newtonian relations. The numerical simulation of hemodynamic flow needs the relationship between viscosity and shear rate. If one considers only the shear-rate-dependent viscosity of blood, then various constitutive equations developed to relate the shear stress tensor and the rate of deformation tensor could be utilized. The non-Newtonian viscosity of normal whole blood, measured by various investigators [14], is shown in Fig. 5 as a function of the shear rate.
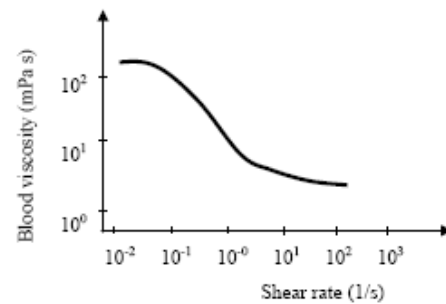

Fig. 5 Blood viscosity vs. Shear rate

In blood flow where the shear rates are not too low, the Casson's relation, based on the dynamic viscosity

measurements is employed in this system. The dominant factor affecting the behavior of blood as a suspension having the aggregatable particles corresponds to the shear thinning effect at increased shear rate. The blood viscosity is derived as a function of the volume rate of particles-hematocrits, and of the shear strain rate. The generalized Casson relation is,

$$\sqrt{\tau} = k_0(c_h) + k_1(c_h)\sqrt{2\sqrt{D_{\mathrm{II}}}} \tag{7}$$

where k_0 and k_1 are parameters depending on the volume fraction of particles in the suspension c_h and D_{Π} is the second invariant of the strain rate tensor;

$$D_{\mathrm{II}} = \frac{1}{2} d_{ij} d_{ij} \tag{8}$$

with the strain rate components d_{ij} given as;

$$d_{ij} = \frac{1}{2}\left(\frac{\partial v_i}{\partial x_j} + \frac{\partial v_j}{\partial x_i}\right), \, i, j = 1,2,3 \tag{9}$$

Finally, the dynamic viscosity μ is expressed as;

$$\mu = \frac{1}{2\sqrt{D_{II}}}\left(k_o(c) + k_1(c)\sqrt{2\sqrt{D_{II}}}\right)^2 \tag{10}$$

3.2 Finite Element Formulation

The mixed velocity-pressure (v-p) and the penalty finite element formulations were used to solve the nonlinear Navier Stokes equations. The advantage of the first formulation is that the pressure, velocity, velocity gradient and stress boundary conditions can be directly incorporated into the finite element matrix equations. The procedure of deriving the element equations relies on the Galerkin method, where the velocity and pressure fields are interpolated over the finite element. The penalty finite element formulation on the other hand has a better conditioning of the discretized system and also reduced number of degrees of freedom, since now only the velocities are the unknown variable. The pressure is eliminated at the element level through the static condensation.

A 21/8 node three-dimensional brick element (i. e. rectangular element) was used for this three-dimensional analysis. 21 nodes were employed to interpolate the velocities and 8 nodes were employed to interpolate the pressure, hence, providing stable elements expressed by the inf-sup condition of Brezzi-Babuska. The finite element mesh of the models consists of 7,200 elements and 8,450 nodes.

3.2.1 Finite element model equations for rigid wall models

The incremental-iterative form of the equation for the time step and the equilibrium iteration "m" are;

$$\begin{bmatrix} \frac{1}{\Delta t}\mathbf{M}_{\mathbf{v}} + {}^{t+\Delta t}\mathbf{K}_{\mathbf{vv}}^{(m-1)} + {}^{t+\Delta t}\mathbf{K}_{\mu\mathbf{v}}^{(m-1)} + {}^{t+\Delta t}\mathbf{J}_{\mathbf{vv}}^{(m-1)} & \mathbf{K}_{\mathbf{vp}} \\ \mathbf{K}_{\mathbf{vp}}^{\mathbf{T}} & \mathbf{0} \end{bmatrix} \begin{Bmatrix} \Delta\mathbf{v}^{(m)} \\ \Delta\mathbf{p}^{(m)} \end{Bmatrix} = \begin{Bmatrix} {}^{t+\Delta t}\mathbf{F}_{\mathbf{v}}^{(m-1)} \\ {}^{t+\Delta t}\mathbf{F}_{\mathbf{p}}^{(m-1)} \end{Bmatrix}$$

$$\tag{11}$$

where the matrices and vectors are,

$$\left(\mathbf{M}_{\mathbf{v}}\right)_{i\alpha\beta} = \rho\int_{V} H_{\alpha} H_{\beta}\, dV = \rho\int_{V}\mathbf{H}^{T}\mathbf{H}\, dV$$

$${}^{t+\Delta t}\left(\mathbf{K}_{\mathbf{vv}}\right)_{i\alpha\beta}^{(m-1)}$$
$$= \rho\int_{V} H_{\alpha} H_{\gamma}{}^{t+\Delta t}v_{j\gamma}^{(m-1)} H_{\beta,j}\, dV$$
$$= \rho\int_{V}\mathbf{H}^{\mathbf{T}}(\mathbf{H}^{t+\Delta t}\mathbf{v}^{(m-1)})\nabla^{T}\mathbf{H}\, dV$$

$${}^{t+\Delta t}\left(\mathbf{K}_{\mu\mathbf{v}}\right)_{i\alpha\beta}^{(m-1)} = \int_{V}\mu H_{\alpha,j} H_{\beta,j}\, dV = \int_{V}\mu\nabla\mathbf{H}^{T}\nabla^{T}\mathbf{H}\, dV$$

$${}^{t+\Delta t}\left(\mathbf{J}_{\mathbf{vv}}\right)_{j\alpha\beta}^{(m-1)}$$
$$= \rho\int_{V} H_{\alpha} H_{\gamma,j}{}^{t+\Delta t}v_{i\gamma}^{(m-1)} H_{\beta}\, dV$$
$$= \rho\int_{V}\mathbf{H}^{\mathbf{T}}(\nabla\mathbf{H}^{t+\Delta t}\mathbf{v}^{(m-1)})\mathbf{H}\, dV$$

$$\left(\mathbf{K}_{\mathbf{vp}}\right)_{i\alpha\delta} = -\int_{V} H_{\alpha,i} G_{\delta}\, dV = -\int_{V}\nabla\mathbf{H}^{T}\mathbf{G}\, dV$$

$${}^{t+\Delta t}\mathbf{F}_{\mathbf{v}}^{(m-1)}$$
$$= {}^{t+\Delta t}\mathbf{R}_{\mathbf{B}} + {}^{t+\Delta t}\mathbf{R}_{\mathbf{S}}^{(m-1)} - \left({}^{t+\Delta t}\mathbf{K}_{\mathbf{vv}}^{(m-1)} + {}^{t+\Delta t}\mathbf{K}_{\mu\mathbf{v}}^{(m-1)}\right){}^{t+\Delta t}\mathbf{v}^{(m-1)} - \mathbf{K}_{\mathbf{vp}}{}^{t+\Delta t}\mathbf{p}^{(m-1)}$$

$${}^{t+\Delta t}\mathbf{F}_{\mathbf{p}}^{(m-1)} = -\mathbf{K}_{\mathbf{vp}}^{T}\,{}^{t+\Delta t}\mathbf{v}^{(m-1)}$$

$${}^{t+\Delta t}\left(\mathbf{R}_{\mathbf{B}}\right)_{i\alpha} = \int_{V} H_{\alpha}{}^{t+\Delta t}f_{i}^{B}\, dV = \int_{V}\mathbf{H}^{T}{}^{t+\Delta t}\mathbf{f}^{\mathbf{B}}\, dV$$

$$^{t+\Delta t}\left(\mathbf{R_S}\right)_{i\alpha}^{(m-1)}$$
$$= \int_S H_\alpha \left(-^{t+\Delta t}p^{(m-1)}n_i + ^{t+\Delta t}v^{(m-1)}{}_{i,j}\,n_j\right)dS$$
$$= \int_S \mathbf{H}^T \left(-^{t+\Delta t}p^{(m-1)}\mathbf{n} + \nabla^{t+\Delta t}\mathbf{v}^{(m-1)}\cdot\mathbf{n}\right)dS$$

$$(12)$$

The left upper index $t+\Delta t$ denotes that the quantities are evaluated at the end of time step. V and S are the volume and the surface of the finite element, respectively. The matrix $\mathbf{H}$ and $\mathbf{G}$ contains the interpolation functions for the velocities and the pressure, respectively. The matrix $\mathbf{M_v}$ is mass matrix, $\mathbf{K_{vv}}$ and $\mathbf{J_{vv}}$ are convective matrices, $\mathbf{K_{\mu v}}$ is viscous matrix, $\mathbf{K_{vp}}$ is pressure matrix and $\mathbf{F_v}$ and $\mathbf{F_p}$ are forcing vectors.

In the penalty formulation the incompressibility condition is used;

$$v_{i,i} + \frac{p}{\lambda} = 0$$

$$(13)$$

where λ is a very large positive scalar so that p/λ is numerically zero for practical purposes. The pressure is calculated as;

$$p = -\lambda v_{i,i}$$

$$(14)$$

Therefore, only the velocities are used in the final finite element matrix equation;

$$\left(\begin{array}{l}\dfrac{1}{\Delta t}\mathbf{M_v} + ^{t+\Delta t}\mathbf{K_{vv}}^{(m-1)} + ^{t+\Delta t}\mathbf{K_{\mu v}}^{(m-1)} \\ + ^{t+\Delta t}\hat{\mathbf{K}}_{\mu v}^{(m-1)} + ^{t+\Delta t}\mathbf{J_{vv}}^{(m-1)} + \mathbf{K_{\lambda v}}\end{array}\right)\Delta\mathbf{v}^{(m)} = ^{t+\Delta t}\hat{\mathbf{F}}_\mathbf{v}^{(m-1)}$$

$$(15)$$

where the matrices are;

$$^{t+\Delta t}\left(\hat{\mathbf{K}}_{\mu v}\right)_{j\alpha\beta}^{(m-1)} = \int_V \mu H_{\alpha,j}H_{\beta,i}\,dV$$

$$\left(\mathbf{K_{\lambda v}}\right)_{j\alpha\beta} = \lambda\int_V H_{\alpha,i}H_{\beta,j}\,dV$$

$$^{t+\Delta t}\hat{\mathbf{F}}_\mathbf{v}^{(m-1)}$$
$$= ^{t+\Delta t}\mathbf{R_B} + ^{t+\Delta t}\hat{\mathbf{R}}_\mathbf{S}^{(m-1)} -$$
$$\left(\begin{array}{l}^{t+\Delta t}\mathbf{K_{vv}}^{(m-1)} + ^{t+\Delta t}\mathbf{K_{\mu v}}^{(m-1)} + \\ ^{t+\Delta t}\hat{\mathbf{K}}_{\mu v}^{(m-1)} + \mathbf{K_{\lambda v}}\end{array}\right)^{t+\Delta t}\mathbf{v}^{(m-1)}$$

$$^{t+\Delta t}\left(\hat{\mathbf{R}}_\mathbf{S}\right)_{i\alpha}^{(m-1)}$$
$$= \int_S H_\alpha\left[\lambda^{t+\Delta t}v^{(m-1)}{}_{j,j}n_i + \left(\begin{array}{l}^{t+\Delta t}v^{(m-1)}{}_{i,j} + \\ ^{t+\Delta t}v^{(m-1)}{}_{j,i}\end{array}\right)n_j\right]dS$$

$$(16)$$

3.2.2 Finite element model equations for deformable wall models

The finite element model equation corresponding to the ALE form of the momentum and continuity equations are a system of ordinary differential equations in the form of;

$$\left(^t\mathbf{M}_{(1)}\mathbf{V}^* + ^t\mathbf{K}_{(1)_w}\Delta\mathbf{V} + ^t\mathbf{K}_{vp}\Delta\mathbf{P} = ^{t+\Delta t}\mathbf{F}_{(1)} - ^t\mathbf{F}_{(1)}\right)\quad(17)$$

and

$$\left(^t\mathbf{M}_{(2)}\mathbf{V}^* + ^t\mathbf{K}_{(2)_w}\Delta\mathbf{V} + = ^{t+\Delta t}\mathbf{F}_{(2)} - ^t\mathbf{F}_{(2)}\right)\quad(18)$$

where additional terms are;

$$\left\{\mathbf{F_1^{ALE}}\right\}_{i\alpha} = \rho\int_V H_\alpha \Delta u_{k,k}^m\,dV$$

$$\left\{\mathbf{F_2^{ALE}}\right\}_{i\alpha} = \rho\int_V H_\alpha\left[\begin{array}{l}-\Delta v_j^m v_{i,j} + \\ \left(v_j - v_j^m\right)\left(\begin{array}{l}v_{i,j}\Delta u_{k,k}^m - \\ v_{i,k}\Delta u_{k,j}^m\end{array}\right)\end{array}\right]dV$$

$$\left\{\mathbf{F_3^{ALE}}\right\}_{i\alpha} = \int_V\left(H_{\alpha,i}p\Delta u_{k,k}^m - H_{\alpha,k}p\Delta u_{k,i}^m\right)dV$$

$$\left\{\mathbf{F_4^{ALE}}\right\}_{i\alpha} = \int_V \mu\left[\begin{array}{l}-H_{\alpha,k}v_{i,j}\Delta u_{k,j}^m + \\ H_{\alpha,j}\left(\begin{array}{l}v_{i,j}\Delta u_{k,k}^m - \\ v_{i,k}\Delta u_{k,j}^m\end{array}\right)\end{array}\right]dV$$

$$\left\{\mathbf{F_5^{ALE}}\right\}_{i\alpha} = \int_S H_\alpha\left\{\begin{array}{l}-p\left(\begin{array}{l}\Delta u_{k,l} \\ -\Delta u_{k,k}^m\end{array}\right)n_i + \\ \mu\left[\begin{array}{l}-v_{i,k}\Delta u_{k,j}^m + \\ v_{i,j}\left(\begin{array}{l}\Delta u_{k,l} - \\ \Delta u_{k,k}^m\end{array}\right)\end{array}\right]n_j\end{array}\right\}dS$$

$$\left\{\mathbf{F_6^{ALE}}\right\}_\delta = \int_V H_\delta\left(v_{i,i}\Delta u_{k,k}^m - v_{i,k}\Delta u_{k,i}^m\right)dV$$

$$(19)$$

4. RESULTS

4.1 Abdominal Aortic Aneurysm Modeling

4.1.1 Rigid wall model

An AAA at the straight aorta domain, where aortas proximal and distal to the AAA bulge are idealized as straight rigid tube and branching arteries are excluded was analysed. The model has ratio D/d=2.75 [15] and geometry generated according to Fig. 1 (D and d are diameters of the bulge and aorta, respectively). The input data used for this simulation are; (a) blood density is ρ=1.05g/cm^3, (b) kinematic viscosity (Newtonian fluid) ν=0.035cm^2/s, and (c) d=12.7mm. The inflow velocity is defined by the flux function given in Fig. 2. The FE mesh consisted of approximately 8000 3D 8-node brick elements.

The results for the velocity and pressure at peak systole t/T=0.16 are shown in Fig. 6. The velocity disturbance in the region of the aneurysm is notable. Also, the region of maximum pressure is located inside AAA.
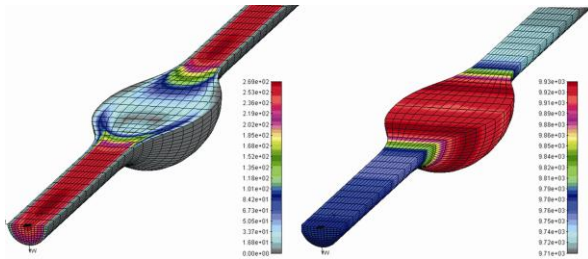

Fig. 6 Velocity field (left panel) and pressure distribution (right panel) for peak systole t/T=0.16 of AAA for the model with D/d=2/75, d=12.7mm.

4.1.2 Deformable wall model

Here, an aneurysm of the straight aorta with deformable walls is modeled according to the fluid-structure interaction algorithm. Blood flow is calculated using 2112 eight-node 3D elements, and 264 four-node shell elements used to model the aorta wall, with the wall thickness δ=0.2cm. The material constants for blood are as in section 4.1.1 while data for the vessel wall are; (a) Young's modulus E = 2.7MPa, (b) Poisson's ratio ν=0.45, (c) wall thickness δ=0.2cm, (d) tissue density ρ =1.1g/cm^3. Boundary conditions for the model are prescribed velocity profile and output pressure profile as shown in Fig. 7(a) and 7(b), respectively [16].

The results for velocity magnitude distribution at t=0.305s are shown in Fig. 8(a). The von Mises wall stress distributions at t = 0.4s is given in Fig. 8(b). It can be seen that the velocities are low in the domain of the aneurysm, while the larger values of the wall stress are at the proximal and distal aneurysm zones.
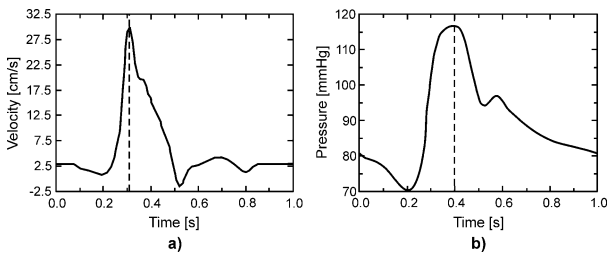

Fig. 7 Input velocity and output pressure profiles for the AAA on a straight vessel. Inlet peak systolic flow is at t=0.305s and outlet peak systolic pressure is at t=0.4s. **a)** Velocity waveform; **b)** Pressure waveform.
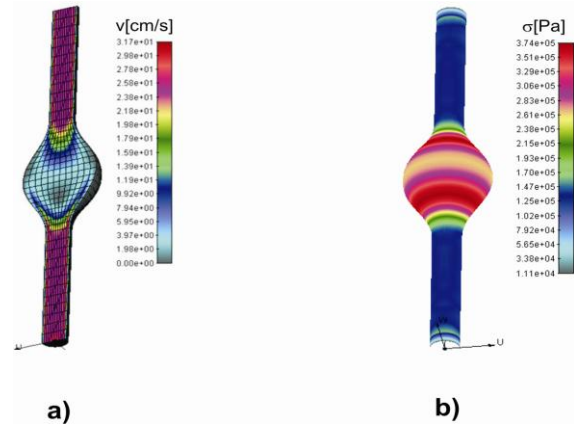

Fig. 8 Velocity magnitude field and von Mises wall stress distribution for symmetric AAA on the straight vessel. **a)** Velocity field distribution for peak at t=0.305s; **b)** von Mises wall stress distributions for blood pressure peak at t = 0.4s.

4.2 Carotid Artery Bifurcation Aneurysm Modelling

4.2.1 Rigid wall model

The FE model is generated using the software based on Fig. 3. The data used for this simulation example are as follows; (a) blood density is ρ=1.05g/cm^3; (b) kinematic viscosity is ν=0.035cm^2/s, (c) geometrical data – diameter of the CCA = 6.2mm, length of the CCA = 7.44mm, diameter of the ICA = 6.5mm, length of the ICA = 26.04mm, diameter of the ECA = 3.658mm, length of the ECA = 18.6mm, diameter to the ICB = 6.5mm, distance to the ICB = 5.39mm, diameter at end of ICA = 4.34mm; angle between ICA and CCA = 25^0, angle between ECA and CCA =25^0. The normal physiological pulsatile waveform form given in Fig. 4(b) is used for the input velocity profile.

An example of the result for the velocity field at diastolic flow is shown in Fig. 9. A stagnation zone of flow is observed at the carotid bulbus distal to the bifurcation region along the internal carotid artery. The atherosclerosis appears in this region in more than 90% cases [8], therefore determination of the stagnation regions within the flow field can be of use in clinical practice.
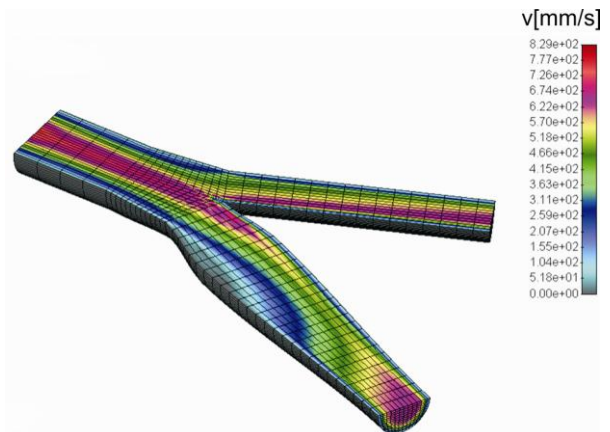

Fig. 9 3D field of velocity magnitude at the maximum systolic flow (at relative time t/T = 0.11 within the period T).

4.2.1 Deformable wall model

Here, blood flow within the bifurcation, including deformation of the vessel walls was modeled. The walls are modeled by the 4-node shell finite elements. Typical geometrical and material data, and flow conditions are used [10]. Geometrical data, with lengths in [*mm*] are; diameter of CCA = 6.0, length of the CCA = 7.0, diameter of ICA = 6.5, length of ICA = 26, diameter of ECA = 3.6, length of the ECA = 18.0, diameter to ICB = 6.5, distance to ICB = 5.3, diameter at end of ICA = 4.0; angle between ICA and CCA = 25^0, angle between ECA and CCA =25^0. Material data for the blood are; (a) density ρ=1.05*g/cm³*, and (b) dynamic viscosity μ=0.0365*P*. Material data for the vessel walls are; (a) Young's modulus $E = 0.361MPa$, (b) Poisson coefficient v=0.45, (c) tissue density ρ =1.1g/cm^3. Wall thicknesses (in [*cm*]) of: CCA = 0.031, distal part (inner carotid wall) = 0.022, outer carotid= 0.02.

Some of the results, which are commonly given in the literature and for certain pulse phase angles during the cycle were presented. These phase angles (relative times) are; (a) systolic peak flow, t/T=0.10; (b) systolic deceleration flow, t/T =0.125; (c) diastolic minimum flow, t/T =0.325; (d) diastolic flow, t/T =0.775.

The effective von-Mises wall stress distribution at several relative times is shown in Fig. 10. It can be seen that the maximum stresses occur in the region of the bifurcation are larger during systole.
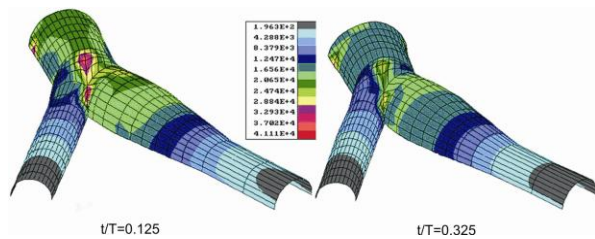

Fig. 10 Distribution of von Mises stress, *Pa* within the artery walls of the carotid artery bifurcation due to action of blood, for systolic deceleration flow, t/T=0.125 and diastolic minimum flow, t/T=0.325.

The shear stress fields are shown in Fig. 11. As can be seen from the figure, the shear stresses are much higher at carotid branch than in the common, external and internal carotid artery. Also, shear stresses are much larger during systole than during diastole.
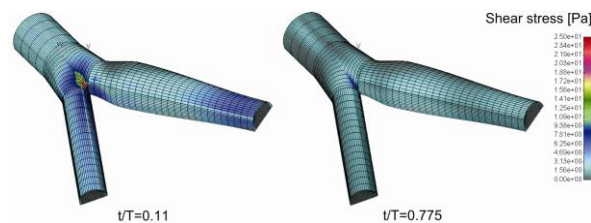

Fig. 11 Wall shear stress field at two relative times (left panel – systole; rigth panel – diastole). Systolic shear stresses are much larger than diastolic

Changes of the axial velocity component at the outer sinus wall position within the cycle are shown in Fig. 12. The solutions are obtained assuming rigid and deformable walls. It can be seen that wall deformation has an influence on

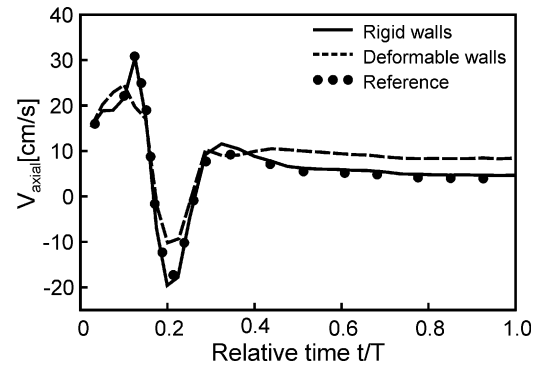velocity, but differences are form around 5% to 10%, that are in good agreement with other literatures [17-18].

Fig. 12 Axial velocity component at the outer sinus wall position during a cycle period, with rigid and deformable walls.

5. DISCUSSION

This work offers a first-generation vascular-surgical simulation for aneurysms. It requires vascular surgeons to be quite familiar with computers, and with computational mechanics to interpret the results of the output data generated by this software. This is a limitation of the current system because any surgical software simulation must be easy to use and to interpret the clinical significance of the results. An additional work is necessary to produce a system that performs well in this respect.

The second limitation is the amount of time required to complete the simulation. Each of the simulation requires about 12 hours of run-time for 3 cycles. The current hardware precludes the surgeon from interacting in real-time with the simulation. With rapidly-increasing speed of computers the real-time should be possible in the near future.

One of the possibilities to make the software usable with today's hardware is to implement parallel computing. Parallel processing is often used for the analysis of large scale problems. For this purpose, a model is decomposed into sub-domains and the analysis is performed on each sub-domain by one processor. The solutions are condensed and combined for the overall solutions, leading to a drastic reduction of the computing time.

From a clinical point of view, it is difficult to develop a universal expert system for diagnostic purposes. The above discussions indicate some possibilities in this direction. A schematic representation of a future expert system is shown in Fig. 13. After a few geometrical measurements from medical devices such as Doppler ultrasound, CAD systems of software provide automatic solid model which then moves on to automatic finite element mesh and numerical calculations. After numerous numerical, experimental and clinical studies, this expert system should have a large database on which some artificial intelligence system (neural network, fuzzy logic, genetic algorithm, etc) could be applied. The medical doctor is not excluded through this software process but he would be even more involved in clinical aspects and predictive medicine rather than routine clinical examinations.
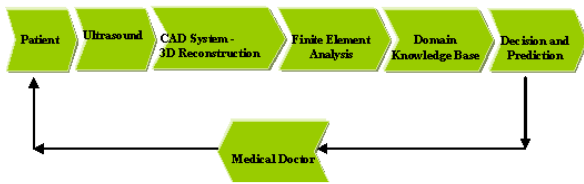
Fig. 13 Expert system for decision-making in medicine.

6. CONCLUSION

The developed a specialized computer software system that functions under the finite element methodologies that support medical investigations of hemodynamic conditions in abdominal aortic and carotid artery bifurcation aneurysms. The developed software applies essential methodologies in numerical procedures such as creating mathematical models, input data preparations, model discretizations, numerical modeling and post-processing options of the aneurismal models. It is important to note that the information provided by the computer simulations of blood flow provides only a portion of data which are needed to design a treatment plan. Other factors, including the morbidity and mortality of the pocedure must be considered. With this in mind, the clinical application of the numerical modeling and development of predictive methods will occupy scientists and biomedical engineers for many years to come.

7. REFERENCES

[1] Cotran, R.S., Kumar. V. and Robbins, S.L. 1994 Robbins pathologic basis of decease. Chapter 11, 499-504, Saunders, London.

[2] Newman, A.B., Arnold, A.M., Burke, G.L., O'Leary, D.H., and Manolio, T.A. 2001 Cardiovascular disease and mortality in older adults with small abdominal aortic aneurysms detected by ultrasonography: the cardiovascular health study. *Annals of Internal Medicine*, 134, 182-190.

[3] Clement Kleinstreuer, and Zhonghua Li. 2006 Analysis and computer program for rupture-risk prediction of abdominal aortic aneurysm. *BioMedical Engineering OnLine*, 5:19.

[4] Myers, K., Devine, T., Barras, C. and Self G. 2001 Endoluminal versus open repair for abdominal aortic aneurysms. http://www.fac.org.ar/scvc//llave/interven/myers/myersi.htm.

[5] Limet, R., Sakalihassan, N., and Albert, A. 1991 Determination of the expansion rate and incidence of rupture of abdominal aortic aneurysms. *Journal of Vascular Surgery*, 14, 540-548.

[6] Fillinger, M.F., Raghavan, M.L., Marra, P., Cronenwett, L. and Kennedy E. 2002 In vivo analysis of mechanical wall stress and abdominal aortic aneurysm rupture risk. *Journal of Vascular Surgery*, 36, 589-596.

[7] Fillinger, M.F., Raghavan, M.L., Marra, P.S. and Kennedy, E.F. 2003 Prediction of rupture in abdominal aortic aneurysm during observation: wall stress vs diameter. *Journal of Vascular Surgery*, 37, 724-732.

[8] Strandness, D. E., and Eikelboom, B. C. 1998 Carotid artery stenosis-where do we go from here? European J. Ultrasound, 7, 17-26.

[9] Ku, D. N. 1997 Blood flow in arteries, Annu. Rev. Fluid Mech. 29, 399-434.

[10] Perktold, K., Resch, M., and Peter, R. O. 1991 Three-dimensional numerical analysis of pulsatile flow and wall shear stress in the carotid artery bifurcation model, *J. Biomechanics*, 24, 409-420.

[11] Cokelet, G. 1987 The rheology and tube flow of blood. In: Skalak R. & Chen S., (eds.) Handbook of Bioengineering, New York: McGraw-Hill.

[12] Sadeghipour, M. and Hajari B. 1995 The pulsatile blood-flow in deformable vessels – non Newtonian behavior. In: Hochmuth R., Langrana N., Hefy M., *(Eds) Proceedings of 1995 Bioengineering Conference, BED*, 29, ASME.

[13] Quarteroni, A., Tuveri, M., and Veneziani, A. 2000 Computational vascular fluid dynamics: problems, models and methods. *Comp. Visual Sci.*, 2, 163-197.

[14] Cho, Y. J., and Kensey, K.R. 1991 Effects of the non-Newtonian viscosity of blood on flows in a diseased arterial vessel. Part 1: Steady flow. *Biorheology*, 28, 241-262.

[15] Peattie, R. A., Riehle, T. J., and Bluth, E. I. 2005 Pulsatile flow in fusiform models of abdominal aortic aneurysms: flow fields, velocity patterns and flow-induced wall stresses, J. Biomech. Eng., 126, 438-446.

[16] Christine M. Scotti, Alexander D. Shkolnik, Satish C. Muluk, and Ender A. Finol 2006 Fluid-structure interaction in abdominal aortic aneurysms: effects of asymmetry and wall thickness, *BioMedical Engineering OnLine*, 4:64.

[17] Perktold, K., and Rappitsch, G. 1995 Computer simulation of local blood flow and vessel mechanics in a compliant carotid artery bifurcation model, *J. Biomechanics*, 28, 845-856.

[18] Filipovic, N., and Kojic, M. 2004 Computer simulation of blood flow with mass transport through the carotid artery bifurcation. *Theoret. Appl. Mech*. 31 (1), 1-33.

[19] Kojic, M., Filipovic, N., Zivkovic, M., Slakovic, R. and Grujovic, N. 1999 PAK-F finite element program for laminar flow of incompressible fluid and heat transfer. *Laboratory of Engineering Software, Faculty of Mechanical Engineering, University of Kragujevac*.

[20] Kojic, M., Filipovic, N., Zivkovic, M., Slavkovic, R., and Grujovic, N. 1998 PAK-FS Finite Element Program for Fluid-Structure Interaction. Faculty of Mech. Engrg, University of Kragujevac, (1998), Serbia.